Automatic Lung Lobe Segmentation of COPD Patients using Iterative B-Spline Fitting

D.P. Shamonin[a], M. Staring[a], M.E. Bakker[a], C. Xiao[b], J. Stolk[c], J.H.C. Reiber[a] and B.C. Stoel[a]

[a]Division of Image Processing, Department of Radiology, Leiden, The Netherlands
[b]College of Electrical and Information Engineering, Hunan University, China
[c]Department of Pulmonology, Leiden, The Netherlands

ABSTRACT

We present an automatic lung lobe segmentation algorithm for COPD patients. The method enhances fissures, removes unlikely fissure candidates, after which a B-spline is fitted iteratively through the remaining candidate objects. The iterative fitting approach circumvents the need to classify each object as being part of the fissure or being noise, and allows the fissure to be detected in multiple disconnected parts. This property is beneficial for good performance in patient data, containing incomplete and disease-affected fissures.

The proposed algorithm is tested on 22 COPD patients, resulting in accurate lobe-based densitometry, and a median overlap of the fissure (defined 3 voxels wide) with an expert ground truth of 0.65, 0.54 and 0.44 for the three main fissures. This compares to complete lobe overlaps of 0.99, 0.98, 0.98, 0.97 and 0.87 for the five main lobes, showing promise for lobe segmentation on data of patients with moderate to severe COPD.

Keywords: lobes segmentation, B-spline fitting, COPD

1. INTRODUCTION

Global lung densitometry using computed tomography (CT) has been established as a sensitive and specific measurement for progression of Chronic Obstructive Pulmonary Disease (COPD), including emphysema. Research is currently focused more on measuring *local* changes in emphysema. In the early development of local measurements, CT scans of the lungs have been divided into separate partitions stacked cranio-caudally.[1] From these partitions, a rough estimation was given on the predominant location of emphysema (basal or apical). Densitometry for each lung lobe separately would facilitate a more specific measure for local progression, since emphysema may be confined to one lobe only. Planning of surgical procedures in the treatment of end-stage COPD, such as lung volume reduction by surgery or by placement of endobronchial devices[2,3] or biodegradable agents, could be made more effective if more localized information could be provided on the lobes.

Existing methods on detecting lung lobes have been based on the watershed method,[4] atlas-based segmentation[5] and implicit surface fitting.[6] These methods may yield fairly accurate results in relatively healthy lungs. However, especially in severe COPD, CT scans may show confounding structures (fibrous tissues resembling fissures), and many incomplete fissures. In those situations, which are clinically of the most interest, watershed methods cannot be expected to perform well. Atlas-based methods may perform better, but they depend on multiple accurate inter-patient registrations, which is time-consuming. Surface fitting approaches seem the most promising for this kind of data.

To improve the robustness of lobe segmentation methods for COPD patients, we propose an alternative method to segment lung lobes, based on sheetness filtering, in combination with an iterative B-spline fitting approach. The latter interpolates in areas of missing fissure information and iteratively includes objects most likely to be part of the fissure, which allows detection of the fissure in multiple disconnected parts. In addition the method allows for effective manual correction by providing extra anchor points, a feature essential for clinical use. In this paper, we aimed however at full automation.

Further author information: (Send correspondence to D.S.)
E-mail: d.p.shamonin@lumc.nl, Telephone: +31 71 526 2137

2. METHODS

The proposed automated lobe segmentation method includes four processing stages: complete lung segmentation, identification of fissure object candidates, fissure segmentation by iterative B-spline fitting and labeling of the lobes, using the detected fissures. Lung segmentation is performed using an automated seeded region growing approach and has been described previously.[7] Minor manual editing was done when needed. Steps two and three are detailed in the following sections. The left and right lung are assumed to contain one and two fissures, respectively.

2.1 Fissure identification

Fissure detection is based on i) fissure enhancement, ii) removal of vessels, iii) removal of noise, resulting in fissure object candidates, and iv) object splitting at junctions to detach fibrotic tissues, and to split multiple fused fissures. The process is illustrated in Figure 1, for a right lung, where F_a till F_d are the detected objects after step i) till iv).

i) Fissure enhancement: The definition of the sheetness filter used in this paper is derived from that of Frangi *et al.*,[8] and modified according to the findings of Xiao *et al.* on a vesselness filter,[9] resulting in:

$$\widetilde{F}(\sigma_f, \boldsymbol{x}) = \begin{cases} 0, & \text{if } \lambda_1 + \lambda_2 + \lambda_3 > 0 \\ \exp\left(-\frac{\mathcal{R}_{\mathcal{A}}^2}{2\alpha_f^2}\right) \exp\left(-\frac{\mathcal{R}_{\mathcal{B}}^2}{2\beta_f^2}\right) \left(1 - \exp\left(-\frac{\mathcal{S}^2}{2c_f^2}\right)\right) \exp\left(-\kappa_f \frac{\|\nabla I\|}{\mathcal{S}}\right), \end{cases} \tag{1}$$

where $\mathcal{R}_{\mathcal{A}}, \mathcal{R}_{\mathcal{B}}, \mathcal{S}$ are a plate-, blob-, and structure strength-measure, respectively, as defined by Frangi *et al.*,[8] where the last term is a step-edge suppression adopted from Xiao *et al.*,[9] and with user-defined parameters $\alpha_f, \beta_f, c_f, \kappa_f$. In this paper the sheetness measure has been computed at a single scale $\sigma_f = 1$ mm.

The fissureness response $\widetilde{F}$ is thresholded at $t_{\widetilde{F}}$ to obtain a binary fissure image F_a.

ii) Removing vessel responses: The sheetness filter (1) not only responds to fissures, but unfortunately also to the outer boundary of vessels, since they resemble sheets. A small scale is needed, however, since the fissure is a thin sheet. In order to remove these responses we opt for generating a rough vessel segmentation, which is subsequently subtracted from the sheetness response. A vessel enhancement function $\tilde{V}(\sigma, \boldsymbol{x})$ has been computed in a multi-scale fashion using a filter developed by Xiao *et al.*,[9] with parameters $\alpha_v, \beta_v, \nu_v, \kappa_v$.

The vesselness response $\tilde{V}$ is thresholded using a parameter-free minimum error clustering technique producing V.[10] A binary fissure $F_b(x)$ is then created by removing the binary vessels from the binary sheetness, using $F_b = F_a \wedge \neg V$.

iii) Noise removal: The segmentation $F_b(x)$ not only contains fissures, but also additional noise. Therefore, small objects were removed using a connected components analysis,[11] based on a physical size threshold t_n, resulting in F_c.

iv) Object splitting: The remaining objects F_c consist of fissure pieces, larger parts of noise, and fibrotic tissue attached to fissures. In addition, horizontal and oblique fissures are connected at so-called junction areas. Opposed to a complicated classification of each object, our approach is based on iterative inclusion of candidates. To that end objects were split at junction locations, so that they were considered different tissue types. Voxels are removed from F_c when the junction function $J(\boldsymbol{x}) = |\max \lambda_i| - |\min \lambda_i|$ is smaller than a threshold t_J. This results in an image F_d containing uniquely labeled candidate fissure objects.

2.2 Lobe segmentation by iterative B-spline fitting

Because of the incompleteness of fissures we opted for a solution that interpolates holes and extends boundaries of the detected object. We employed smooth B-spline functions for scattered data approximation.[12,13] First we briefly describe the general B-spline fitting technique, then the iterative inclusion of a subset of the candidate fissure objects F_d, and finally the lobe extraction.

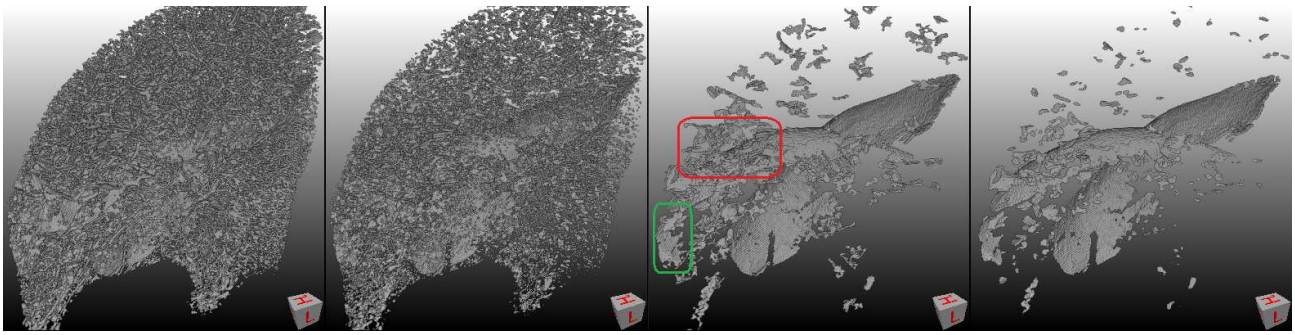

Figure 1. Fissure candidate selection. From left to right: F_a, F_b, F_c and F_d. The red box marks fibrotic tissue attached to the fissure, and the green box an isolated fissure part.

B-spline fitting: Given a set of n point-value pairs $\mathcal{Z} = \{\{\boldsymbol{x}, \text{value}\}_i | i = 1, \ldots, n\}$ with the coordinates located at the fissure candidate objects $F_d(\boldsymbol{x})$, and paired with a value 0, we seek a smooth function F_{spline} that fits the data best in a least square sense. We employed the work of Lee *et al.*,[12] significantly extended by Tustison *et al.*,[13] i.e. in 3D we find the function:

$$F_{\text{spline}}(\boldsymbol{x}) = \sum_{i_0=0}^{O} \sum_{i_1=0}^{O} \sum_{i_2=0}^{O} \boldsymbol{P}_{i_0,i_1,i_2} B_{i_0}^{O}(x_0) B_{i_1}^{O}(x_1) B_{i_2}^{O}(x_2), \tag{2}$$

where B_i^O are the smooth and local B-spline basis functions, $O = 3$ the spline order, and $\boldsymbol{P}$ the control point lattice that need to be solved for such that $F_{\text{spline}}(\boldsymbol{x}) = 0, \forall x \in \mathcal{Z}$. The B-splines are multi-level, with a doubling of the control point resolution in every level.

To avoid the trivial solution $F_{\text{spline}}(\boldsymbol{x}) = 0, \forall \boldsymbol{x}$, we defined additional points around the candidate objects F_d to make sure that $F_{\text{spline}}(\boldsymbol{x}) \neq 0$ for points outside the fissure. These off-fissure points are defined as follows: we take the local normal $\boldsymbol{n}(\boldsymbol{x})$ of a fissure point $\boldsymbol{x}$ and set points at a distance d_{n} along the normal to either 1 or -1: $\boldsymbol{x} \pm d_{\text{n}} \boldsymbol{n}(\boldsymbol{x}) = \pm 1$. The local normal is computed by means of a Principal Components Analysis (PCA) on a $3 \times 3 \times 3$ neighborhood, taking the first principal component as the normal. Then, the off-fissure points and their values (± 1) are added to the set $\mathcal{Z}$, and the control points $\boldsymbol{P}$ are solved such that $F_{\text{spline}}(\boldsymbol{x}) = \text{value}(\boldsymbol{x}), \forall x \in \mathcal{Z}$.

Iterative object inclusion: The candidate fissure objects F_d contain multiple fissure parts and falsely detected objects. Opposed to trying to classify each object, we propose to use an iterative B-spline fitting approach to group objects. First, a B-spline is fitted through the largest object, after which one or more objects are included, until no more objects satisfy the inclusion criteria. Then, for the right lung, we proceed with the next fissure. The procedure is illustrated in Figure 2. For every iteration i, for every currently unassigned (uniquely labeled) object O_j, we define the inclusion criteria as follows:

1. Given the current B-spline fit function F_{spline}^i, we compute the mean fit values $\overline{F}_j = \frac{1}{|O_j|} \sum_{\boldsymbol{x} \in O_j} F_{\text{spline}}^i(\boldsymbol{x})$.
2. The minimum distance to the currently included objects $d_j^{\min}$.

All objects that are close enough and are in alignment with the current estimate are included in the next estimate. In other words, objects that satisfy $\overline{F}_j < t_{\overline{F}}$ and $d_j^{\min} < t_d$ are included, based on two thresholds $t_{\overline{F}}$ and t_d, upon which a new B-spline fit F_{spline}^{i+1} is generated.

Lung lobes labeling: Final lobe labeling for the left lung is based on the sign of the B-spline fit function F_{spline}. For the right lung we have three lobes and two fit functions. Splitting is performed based on the sign of F_{spline} and on the occurrence of objects at the interface. In the very last step the centers of gravity are used to identify superior and inferior lobes.

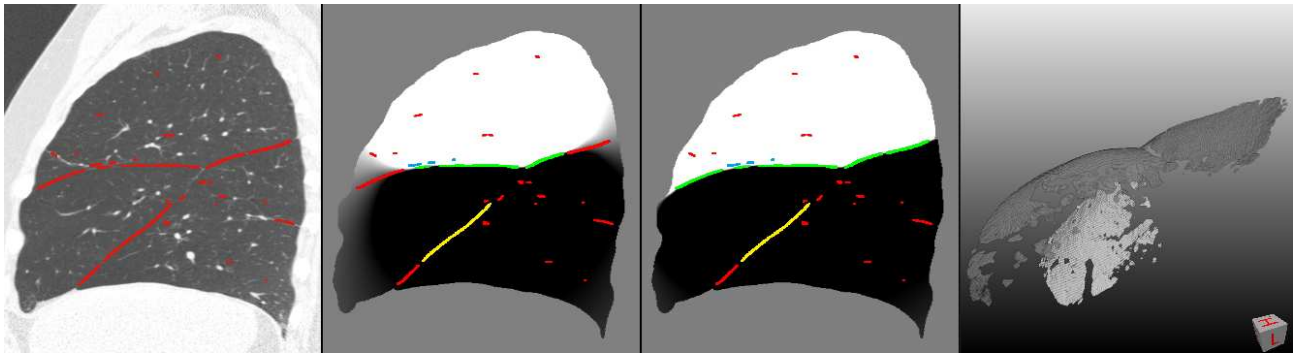

Figure 2. Iterative B-spline fitting. The first image is the input, the next two images show two iterations of the object inclusion, depicting F^0_{spline} and F^1_{spline}. The fissure candidates F_d are overlaid in color, with green the current selection. The yellow label was excluded due to failure to both inclusion criteria ($\overline{F} = -7.6, d^{\min} = 10.7$), whereas the blue label was excluded due to insufficient fit ($\overline{F} = 1.2, d^{\min} = 2.5$). Note the grey regions representing fit insecurity. The last image shows the finally included objects.

3. EXPERIMENTS AND RESULTS

Our algorithm was implemented in the C++ language using the ITK and integrated into MeVisLab. The calculation time for a typical 256x256x512 size dataset is about 6 minutes for the right lung on an HP Z400 (2.66 GHz CPU; 6 GB RAM). The most demanding steps are fissure and vessel enhancement (95 and 38 s.), junction removal (38 s.), and the iterative B-spline fitting (190 s.).

3.1 Data, reference standard, and parameter settings

We used CT images of 23 patients (20 males) from a former study,[14] scanned with a Toshiba Aquilion16 scanner, with the following parameters: 120 kVp; 140 mAs per rotation; rotation time 0.4 s.; collimation: 16 x 0.5 mm; and pitch factor: 1.4375. Images were reconstructed with an FC02 kernel (FOV of 295 - 400 mm; slice thickness 0.5 mm; increment 0.5 mm). Scans were made during breath hold at full inspiration, without contrast media. The patient group had moderate to severe COPD (GOLD stage II and III) without $\alpha 1$ antitrypsin deficiency; aged 49-78, and FEV_1 between 36% and 87% predicted. CT scans frequently showed fibrotic tissues and incomplete fissures, through which veins could pass.

To evaluate the proposed method, ground truth lobe segmentations were generated as follows. First, an initial segmentation was generated by morphological watersheds. Then, one of the authors (M.E.B.) corrected this manually using the software ITK-SNAP.[15] After inspection and approval by a pulmonologist (J.S.) a ground truth for each lobe was established. For one patient it was not possible to create a correct lobe segmentation due to severe destruction of fissures and parenchyma, and this CT scan was therefore excluded.

The segmentation parameters were chosen heuristically. To compute $\widetilde{F}$ we used $\sigma_f = 1$, $\alpha_f = 0.5$, $\beta_f = 0.5$, $c_s = 1$, $\kappa_s = 3$. Parameters for computing the vesselness V were adopted from Xiao *et al.*:[9] $\alpha_v = 0.1$, $\nu_v = 0.3$, $\kappa_v = 0.8$, $\beta_v = 0.5$. Vesselness was computed at scales $\sigma_v = 1, 1.6, 2.5, 4$ mm. Thresholding was parameter-free. Sheetness was thresholded at $t_{\widetilde{F}} = 0.05$, while for the vesselness minimum error thresholding technique we used 128 bins and a Gaussian mixture type. Objects smaller than $t_n = 30$ mm^3 were removed. Object splitting was done with $t_J = 0.5$ and 0.4 for the right and left lung, respectively. Iterative object inclusion was performed with $d_n = 5, t_d = 10$, and $t_{\overline{F}} = 1$, and a control point grid using 8 levels and 4 control points in the first level.

3.2 Evaluation

The overlap between the results of the proposed method and the ground truth was defined by the Dice similarity coefficient (DSC). To better appreciate differences, the overlap was additionally computed on the fissure area. The fissure area was defined as a three voxel wide area around the fissure, computed using the morphological gradient operation on the lobe segmentations. The DSCs are presented by box-and-whisker plots. In addition, we verified the suitability of the proposed method for lobe-based densitometry, by comparing the

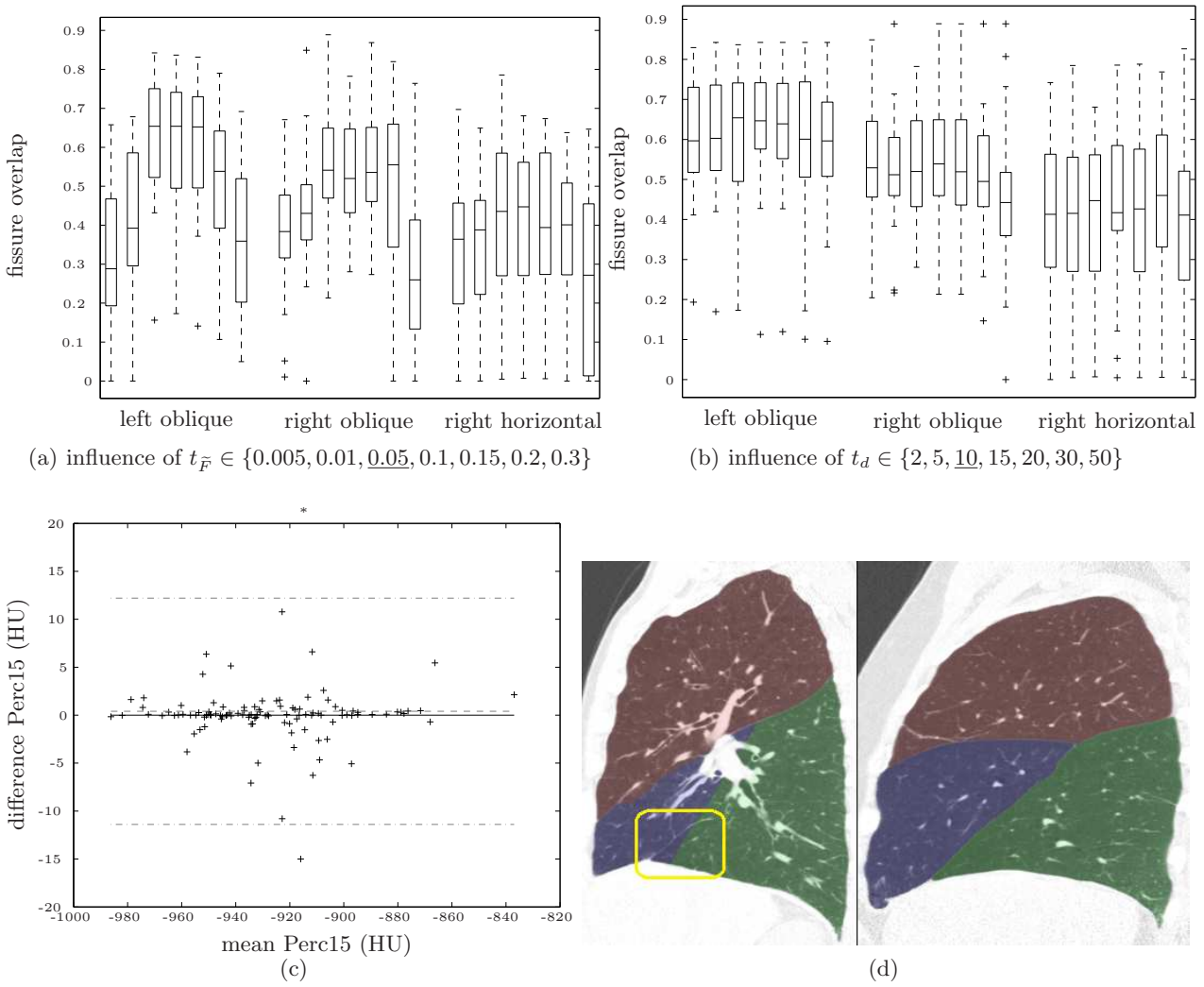

(a) influence of $t_{\widetilde{F}} \in \{0.005, 0.01, \underline{0.05}, 0.1, 0.15, 0.2, 0.3\}$

(b) influence of $t_d \in \{2, 5, \underline{10}, 15, 20, 30, 50\}$

(c)

(d)

Figure 3. Results. Box-plots for the fissure overlap: a) varying $t_{\widetilde{F}}$; b) varying t_d; c) a Bland-Altman plot for lobe-based densitometry using the standard settings (* denotes an outlier > 20 HU; mean difference 0.4 HU; 95% confidence interval $[-11.4, 12.2]$ HU); d) final lobe segmentation examples (with and without error).

automatically determined 15$^{\text{th}}$ percentile point (Perc15) of each lobe with the ground truth. We analyzed the influence of two parameters that have a marked impact on the results: $t_{\widetilde{F}}$ and t_d. The first was varied over $t_{\widetilde{F}} \in \{0.005, 0.01, \underline{0.05}, 0.1, 0.15, 0.2, 0.3\}$ and the second over $t_d \in \{2, 5, \underline{10}, 15, 20, 30, 50\}$, where the underlined values are the chosen settings.

3.3 Results

The proposed lobe segmentation algorithm was tested on the COPD data, with the settings described above. The results for the experiments are given in Figure 3(a) and 3(b), showing the influence of $t_{\widetilde{F}}$ and the relative insensitivity for t_d respectively. For the optimal settings $t_{\widetilde{F}} = 0.05$ and $t_d = 10$ a median overlap of the fissures of 0.65, 0.54 and 0.44 was obtained for the left horizontal, right oblique and right horizontal fissure, respectively. This compares to complete lobe overlaps with the groundtruth of 0.99, 0.98, 0.98, 0.97 and 0.87 for the left superior, left inferior, right superior, right inferior and right middle lobe, respectively. Bland-Altman analysis showed no significant difference in 15$^{\text{th}}$ percentile point between automated and manual segmentation, see Figure 3(c). Figure 3(d) shows an example of the lobe segmentation results.

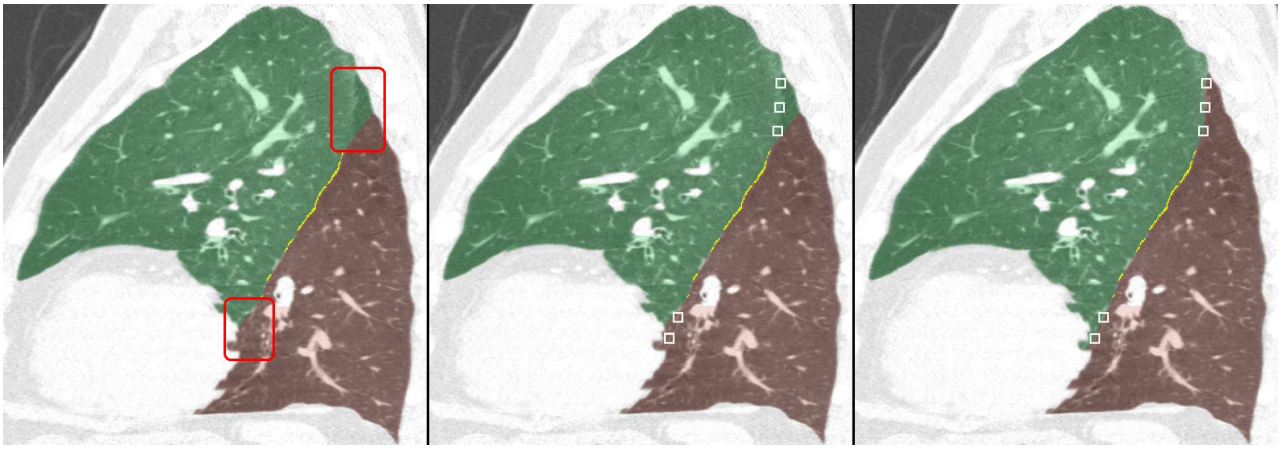

Figure 4. The possibility for user interaction. The left image shows a possible result of the automatic method. The red boxes show a segmentation error. Users can manually add control points to the set $\mathcal{Z}$ by clicking on the image (middle). After hitting an update button the B-spline fit from equation (2) is recomputed, resulting in an updated lobe segmentation (right image). Updating takes about 2 s.

4. CONCLUSIONS AND DISCUSSION

An automatic method for lung lobe segmentation is presented, using B-spline fitting for smooth interpolation across regions with little information, combined with an iterative fissure candidate object inclusion approach to overcome false responses on non-fissure objects and fissures not detected in one piece. The method was demonstrated on data of COPD patients with incomplete fissures, (severely) affected by emphysema, fibrotic tissue mimicking fissures, and vasculature passing through fissures. In addition to these disease-related segmentation problems, CT image artifacts also produced discontinuous fissure appearances, due to cardiac motion.

These challenges put demands on methods. Because of incomplete (-ly detected) fissures, watershed methods can not perform well. Smooth interpolation across detected fissure pieces is necessary. In addition, it cannot be assumed that the fissure is detected in one part, and therefore multiple objects corresponding to the same fissure need to be grouped. In addition, it needs to account for removal of noise and confounding structures.

Compared to the literature the proposed method bears most resemblance with that of Pu *et al.*[6] They used intensity thresholding to detect fissures, without falsely detecting fibrotic tissue, because the HU's differed. In our data, however, the image intensities of the fibrotic tissue and fissures overlapped so that thresholding could not be applied. Pu *et al.* used subsequently the orientation compared to the z-axis to distinguish fissures from other structures. However we found that this orientation can vary too much between patients. Therefore this algorithm would probably not be successful in our data. In addition, we can overcome gaps in the detected candidates by means of the iterative inclusion approach.

The proposed method performs reasonably well, with a median Dice overlap of the fissure boundaries of 0.65, 0.54 and 0.44. As shown in Figure 3(c) the lobe segmentation quality is sufficient for lobe-based densitometry. The proposed method has a practical advantage for clinical use with the inherent capability for easy user-correction. Additional fissure locations could be provided by the user with a few mouse-clicks, after which the lobe segmentation is quickly updated. The procedure is illustrated in Figure 4

The fitting approach is dependent on the selection of candidate fissure objects. In that respect our algorithm will benefit from improved fissure enhancement and noise suppression filters which are work in progress. The inclusion criteria during the iterative fitting may be improved and a number of parameters could be removed by further automation. The PCA-based determination of the normal currently poses problems for spherical objects. Near the hilum, fissure candidates were not always detected due to a jagged appearance caused by cardiac motion, resulting in a low response of the sheetness filter.

In conclusion, we developed an algorithm that shows good overlap with manually segmented lobes in patients with moderate to severe emphysema, within an acceptable computation time.

Acknowledgments

This research was funded by the Dutch Technology Foundation (STW), grant number LPG.07998, under the acronym APPEAR (Assessing the Progression of Pulmonary Emphysema by Advanced Registration). This work benefitted from the use of the Insight Segmentation and Registration Toolkit (ITK), and MeVisLab (MeVis Medical Solutions GmbH, Bremen, Germany).

REFERENCES

1. M. Bakker *et al.*, "Assessment of regional progression of pulmonary emphysema with CT densitometry," *Chest* **134**(5), pp. 931 – 937, 2008.
2. R. Berger and *et al.*, "Lung volume reduction surgery: a meta-analysis of randomized clinical trials," *Treat Respir Med* **4**, pp. 201 – 209, 2005.
3. F. Sciurba *et al.*, "A randomized study of endobronchial valves for advanced emphysema," *N Engl J Med* **363**, pp. 1233 – 1244, 2010.
4. J. Kuhnigk *et al.*, "Lung lobe segmentation by anatomy-guided 3D watershed transform," in *SPIE*, pp. 1482–1490, 2003.
5. E. van Rikxoort *et al.*, "Automatic segmentation of pulmonary lobes robust against incomplete fissures," *IEEE T Med Imaging* **29**(6), pp. 1286–1296, 2010.
6. J. Pu, "Pulmonary lobe segmentation in CT examinations using implicit surface fitting," *IEEE T Med Imaging* **28**, pp. 1986 – 1996, 2009.
7. B. C. Stoel and J. Stolk, "Optimization and standardization of lung densitometry in the assessment of pulmonary emphysema," *Invest Radiol* **39**(11), pp. 681 – 688, 2004.
8. A. Frangi *et al.*, "Multiscale vessel enhancement filtering," in *MICCAI*, *LNCS* **1496**, pp. 130–137, 1998.
9. C. Xiao *et al.*, "A strain energy filter for 3D vessel enhancement with application to pulmonary CT images," *Med Image Anal* **15**(1), pp. 112 – 124, 2011.
10. J. Kittler and J. Illingworth, "Minimum error thresholding," *Pattern Recognition* **19**, pp. 41–47, 1986.
11. G. Lehmann, "Label object representation and manipulation with ITK," *The Insight Journal* , 2007.
12. S. Lee *et al.*, "Scattered data interpolation with multilevel B-splines," *IEEE T Vis Comput Gr* **3**, pp. 228–244, 1997.
13. N. Tustison and J. Gee, "Generalized n-D c^k B-spline scattered data approximation with confidence values," in *MIAR*, pp. 76 – 83, 2006.
14. T. Lapperre *et al.*, "Smoking cessation and bronchial epithelial remodelling in COPD: a cross-sectional study," *Resp Res* **8**(1), p. 85, 2007.
15. P. A. Yushkevich and *et al.*, "User-guided 3D active contour segmentation of anatomical structures: Significantly improved efficiency and reliability," *NeuroImage* **31**(3), pp. 1116 – 1128, 2006.